



ELSEVIER

Earth and Planetary Science Letters 203 (2002) 117–130

EPSL

www.elsevier.com/locate/epsl

Variations in the distribution of magma in the lower crust and at the Moho beneath the East Pacific Rise at 9°–10°N

Wayne C. Crawford^{a,*}, Spahr C. Webb^b

^a *Scripps Institution of Oceanography, University of California, San Diego, La Jolla, CA 92093-0205, USA*

^b *Lamont Doherty Earth Observatory, Columbia University, Palisades, NY 10964, USA*

Received 9 July 2001; received in revised form 8 April 2002; accepted 12 July 2002

Abstract

Measurements of the seafloor deformation under ocean waves (compliance) reveal an asymmetric lower crustal partial melt zone (shear velocity less than 1.8 km/s) beneath the East Pacific Rise axis between 9° and 10°N. At 9°48'N, the zone is less than 8 km wide and is centered beneath the rise axis. The zone shifts west of the rise axis as the rise approaches the westward-stepping 9°N overlapping spreading center discontinuity and is anomalously wide at the northern tip of the discontinuity. The ratio of the compliance determined shear velocity to the compressional velocities (estimated by seismic tomography) suggests that the melt is well-connected in high-aspect ratio cracks rather than in isolated sills. The shear and compressional velocities indicate less than 18% melt in the lower crust on average. The compliance measurements also reveal a separate lower crustal partial melt zone 10 km east of the rise axis at 9°48'N and isolated melt bodies near the Moho beneath four of the 39 measurement sites (three on-axis and one off-axis). The offset of the central melt zone from the rise axis correlates strongly with the offset of the overlying axial melt lens and the inferred center of mantle melting, but its shape appears to be controlled by crustal processes.

© 2002 Elsevier Science B.V. All rights reserved.

Keywords: deformation; shear modulus; deformation velocity; East Pacific Rise; mid-ocean ridges; melts; lower crust

1. Introduction

Petrologic studies indicate that oceanic crust created at magma-rich spreading centers is derived from mantle peridotites by partial melting [1,2], but there is no consensus on how the melt is

focussed to the rise axis or how it travels through and is emplaced in the crust. A key to understanding these processes is to determine how much melt there is in the crust, where it is, and how well connected it is. Seismic studies of the magma-rich East Pacific Rise (EPR) reveal a thin melt sill [the axial magma chamber (AMC) reflector] beneath most of the rise axis at depths between 1.1 and 1.8 km [3–6], and most EPR melt supply models are based on explaining the position and depth of this reflector [7–9]. The best-studied section of the EPR is the segment located between the Clipperton transform at 10°10'N and

* Corresponding author. Present address: Laboratoire de Géosciences Marines, IGP Case 89, 4 Place Jussieu, 75252 Paris, France. Tel.: +33-1-4427-2416; Fax: +33-1-4427-3894.

E-mail addresses: crawford@ipgp.jussieu.fr (W.C. Crawford), scw@ldeo.columbia.edu (S.C. Webb).

an overlapping spreading center (OSC) at 9°03'N (Fig. 1). At the north end of this segment, the AMC reflector is narrow and centered beneath the rise axis, but the reflector widens and extends west of the rise axis as the rise approaches the OSC. The rise axis steps west at the OSC, and to the south the reflector is once again narrow and centered beneath the rise axis. This suggests that the wide AMC just north of the OSC transports melt to the rise axis from a misaligned deep source and that the OSC represents a region where the rise axis is realigned with this deep source [5]. Within the OSC, the AMC reflector is up to 4 km wide and has a complex morphology indicating a local melt supply [10].

The lower crust also plays an important role in melt transport and storage [11,12]. Initially believed to be completely molten at the EPR rise axis, then considered to contain little or no melt [13], the lower crust has recently been shown to contain a narrow (4–6-km-wide) partial melt zone [14]. Seismic tomography studies suggest that compressional velocity increases significantly with depth in this melt zone, suggesting that there is less melt in the lowermost crust than in the mid-crust. Recent models based on ophiolite studies suggest, however, that the lowermost crust forms by periodic emplacement of melt sills [12] derived from melt channels penetrating through the uppermost mantle [15]. These melt sills may create significant seismic anisotropy and a higher measured seismic velocity for a given melt percentage than the potentially better-connected melt in the mid-crust [16].

Seismic studies also image a much wider (15–20 km) melt zone at the top of the mantle. The center (minimum velocity) of this melt zone offsets west of the rise axis as the ridge approaches the 9°03'N OSC from the north and the melt zone is continuous across the OSC [14,17].

To better resolve the amount and distribution of lower crustal melt, we measured seafloor compliance – the seafloor displacement under ocean gravity wave loading – at 39 sites along and across the EPR between 9° and 10°N. Compliance is most sensitive to the crustal shear modulus, which we convert to shear velocity, and is particularly sensitive to low shear velocity regions such

as melt zones. Using these compliance measurements, we estimate the crustal shear velocity, which allows us to determine the melt distribution in the EPR lower crust as well as pure melt bodies at or near the Moho. Shear velocity constraints from compliance measurements complement compressional velocity constraints from seismic methods to improve estimates on melt quantity and distribution. In addition, compliance measurements are quasi-static and so are unaffected by seismic wave attenuation, reflection and diffraction that complicates seismic data in fluid-bearing zones. We compare the crustal shear velocities with compressional velocity estimates from seismic experiments to better constrain the distribution and quantity of melt in these zones.

2. Data analysis

In this paper, we focus on compliance measured on three across-axis lines at 9°48'N, 9°33'N and 9°08'N and along the rise axis from 9°48'N to 9°02'N. We use one-dimensional (1-D) minimum structure inversions to determine what features are required by the data, and we use block model inversions to calculate the best velocity constraints for a given two-dimensional (2-D) structure (see the Appendix). Lower crustal shear velocities below 2.5 km/s require melt [18], while velocities below 1 km/s are assumed to be essentially zero, implying no connected solid matrix [19]. We refer to regions with shear velocities below 1 km/s as 'melt' bodies and those with shear velocities between 1 and 2.5 km/s as 'mush' zones.

The on-axis compliance function at 9°48'N is dominated by two peaks: one broadband and centered at 14 mHz and the other narrowband and centered at 8 mHz (Fig. 2A). A 1-D minimum structure inversion of this compliance indicates two melt zones, one at the depth of the AMC and the other at the depth of the Moho, separated by a lower crustal mush zone (Fig. 2B). The weighted root-mean-square misfit to the data is greater than 1 for this model, indicating that the inversion does not completely fit the data. A 2-D block model inversion does fit the data, for shear velocities less than 0.1 km/s in the melt zones and

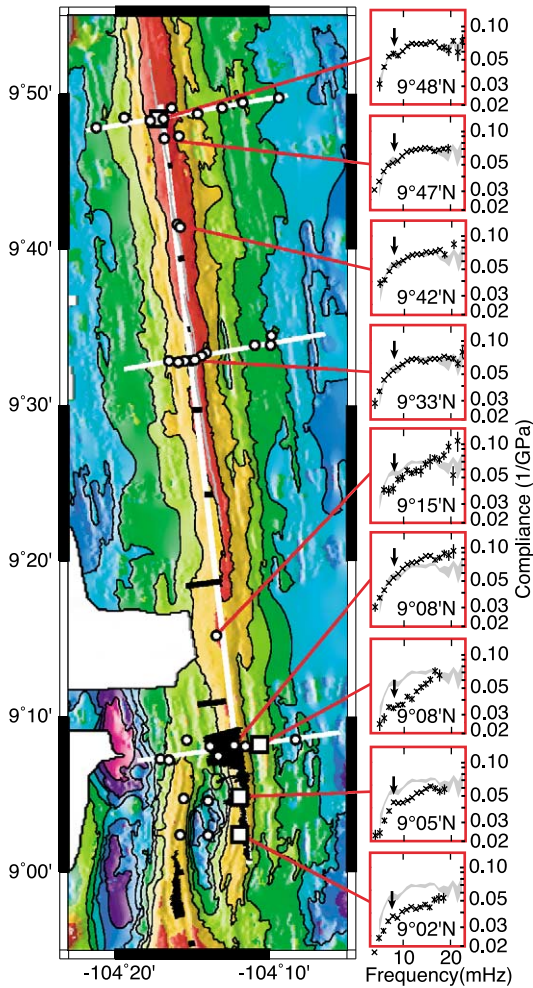


Fig. 1. EPR compliance measurements. Left: Measurement sites. White squares mark sites overlying a Moho melt body (discussed in the text); white circles mark the rest. White lines underline the along- and across-axis lines discussed in the text. Black lines mark the east–west limits of the AMC reflector determined by seismic studies [5,10]. Right: Selected compliances and error bars. The gray region is a reference (on-axis compliance at 9°48'N), and arrows mark the frequency at which a Moho-level melt body would create a peak in compliance.

less than 1.8 km/s on average throughout the lower crust [18].

The Moho melt body generates the narrowband peak at 8 mHz. This peak is only created if shear velocities are slower than 0.1 km/s at or near the Moho. A layer up to 2 km thick can produce this peak (Fig. 3), but such a thick layer is inconsistent

with seismic tomography results which do not image any Moho-level melt body. This peak is best explained as a thin (50–200 m) layer, too small to be tomographically imaged, which corresponds to a shear velocity less than 0.01 km/s. The 8-mHz peak is still present 0.5 km off-axis, but is gone by 1 km off-axis[18], suggesting that the Moho body is less than 2 km wide; the best fit is a melt lens 0.7 km wide. We interpret this body as corresponding to one or more thin melt sills.

Moho melt bodies are indicated by 8-mHz compliance peaks at two other on-axis sites and one off-axis site. The peak is visible in on-axis compliance at 9°48'N, 9°05'N and 9°02'N and in compliance measured 2.5 km east of the rise axis at 9°08'N (Fig. 1). The peak is notably absent on-axis at 9°42'N, 9°33'N and 9°08'N, suggesting that either Moho melt bodies are disconnected or that, if there is a continuous body, its shear velocity varies rapidly along-axis. It may be significant that three of the four sites with clear 8-mHz peaks are located in or near the OSC.

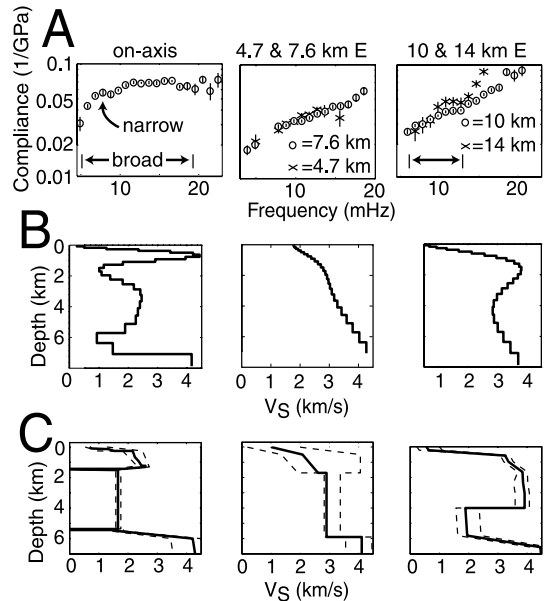


Fig. 2. Shear velocity inversions of compliance data at 9°48'N. Left column = on-axis, middle column = 4.7 and 7.6 km east, right column = 10 and 14 km east (inversions are from 10 km east). (A) Measured compliances and error bars. Arrows indicate compliance peaks discussed in the text. (B) 1-D minimum structure inversions. (C) Block model inversions. Solid lines = best fits; dashed lines = error bounds.

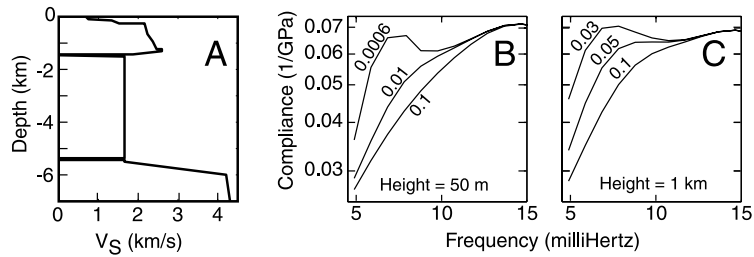


Fig. 3. The effect of Moho-level melt bodies on the compliance function. (A) 9°48'N on-axis model (from [18]). (B) Compliance functions below 15 mHz created by a 50-m thick Moho melt sill. Each curve represents a different sill shear velocity (shown in km/s next to each curve). (C) Same as B, except for a 1-km-tall melt zone centered at the Moho.

The broadband compliance peak centered at 14 mHz is primarily generated by the lower crustal mush zone (the narrowband peak generated by the AMC is more subtle). At 9°48'N, this peak is gone by 4.7 km east of the rise axis (Fig. 2A), indicating that the mush zone is relatively narrow. Ten and 14 km off-axis, however, a smaller and lower-frequency broadband compliance peak appears. Minimum structure inversions of the 9°48'N data reveal a low-velocity zone (LVZ) in the bottom half of the lower crust 10 km off-axis and no such zone 4.7 or 7.6 km off-axis (Fig. 2B). Lower crustal shear velocities determined using block inversions of these data (Fig. 2C) require melt in the 10 km off-axis LVZ ($V_s = 2.0 \pm 0.5$ km/s) but no melt 4.7 and 7.6 km off-axis ($V_s > 2.8$ km/s), suggesting that there are two separate lower crustal mush zones, one centered on-axis and the other starting near 10 km off-axis. The low-frequency peak associated with this off-axis mush zone is even more pronounced 14 km off-axis, but the data uncertainties there are larger so the inversions are not constrained well enough to require a lower crustal mush body. Based on a subset of the 9°48'N data collected in 1994, which contained only the on-axis and 10 km off-axis measurements, Crawford et al. [18] proposed that the lower crustal mush zone is at least 20 km wide. The newer compliance data measured between these sites demonstrate that the melt detected 10 km off-axis is in a separate body that extends to at least 14 km off-axis.

To visualize the distribution of melt and mush in the lower crust, we plot compliance as a function of off-axis distance for the three across-axis lines. We display a contour plot for all measured

frequencies (Fig. 4A) and also across-axis transect at the frequency most sensitive to lower crustal shear velocities (10 mHz, Fig. 4B). At 9°48'N and at 9°33'N, lower crustal compliance is bell-shaped, decreasing rapidly within 2 km of a central peak near the rise axis. This indicates that there is a narrow mush region centered near the rise axis. Lower crustal compliance then increases again beyond 5–7 km east of the rise axis (Fig. 4B), indicating that lower crustal shear velocities reach a maximum within ~ 5 km of the rise axis and then decrease again between 7 and 10 km off-axis. Lower crustal shear velocities must increase further off-axis with the cooling of the crust, but our measurements do not go out far enough to see this.

To determine the variations in lower crustal shear velocity with distance off-axis, we calculated shear velocities using 1-D block models at (1) the near-axis sites with the highest compliance, (2) the 'intermediate' sites with the lowest compliance and (3) the farthest off-axis sites. The block models use a constant-velocity layer in the lower crust, but a positive or negative velocity gradient is also possible [18]. The velocity in each region is remarkably similar at the different latitudes (Fig. 4C). Lower crustal velocities average 1.7–1.8 km/s near the rise axis (indicating mush), 2.8–2.9 km/s beneath the intermediate sites (indicating no melt), and decrease again farther off-axis. At 9°48'N, lower crust shear velocities are as low as 2.0 km/s at 10 km east of the rise axis, requiring melt. At 9°08'N and 9°33'N, lower crustal velocities are 2.6–2.7 km/s at the farthest off-axis sites, approximately 0.2 km/s slower than at the 'intermediate' sites but not low enough to require

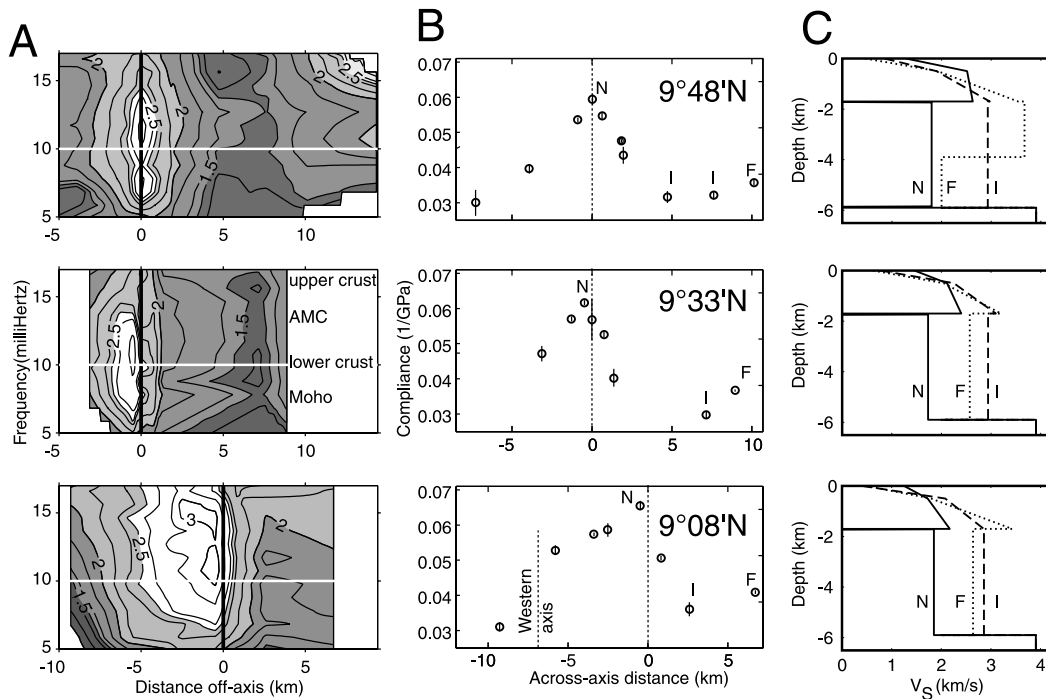


Fig. 4. Measured compliances and best-fit block models. Top row = 9°48'N; middle row = 9°33'N; bottom row = 9°08'N. (A) Contour plot of compliance as a function of frequency and distance from the rise axis, normalized by dividing by compliance of typical young oceanic crust [21]. High compliance (light shades) indicates slow velocities. Black vertical lines mark the rise axis; white horizontal lines mark the frequency of data displayed in column B. The middle plot also indicates the crustal units corresponding to each frequency. (B) 10-mHz compliance with error bars as a function of distance from the rise axis. Dotted vertical lines mark the rise axis. Letters indicate near-axis (N), intermediate (I) and far (F) sites (see text) used to calculate the models shown in C. (C) Best-fitting block models at near-axis, intermediate and far sites.

melt. However, these sites are only 7–9 km east of the rise axis, possibly not far enough to detect the same type of off-axis mush body as that seen 10–14 km off-axis at 9°48'N.

The melt fraction corresponding to the measured shear velocities depends on how the melt is aligned and connected. Well-connected melt in high-aspect ratio features such as films and tubes reduces shear velocities and increases the ratio of compressional to shear velocity more than poorly connected melt in low-aspect ratio bodies such as spheres or small sills [20]. On-axis, the compressional to shear velocity ratio (calculated using the slowest compressional velocity estimates [14]) is greater than 2.1 in the lower crust. Young oceanic lower crust normally has a compressional to shear velocity ratio of 1.7–1.8 [21] and neither heating nor spherical melt inclusions can change this ratio significantly [22]. The lower crustal melt is there-

fore probably in connected films or tubes or in flattened sills. For a film or tube geometry, the shear velocities indicate 2.5–17% melt in the lower crust near the rise axis [18], consistent with estimates of up to 10–16% for a film geometry from tomographic models of compressional velocity [14]. The lower crust shear velocities 10 km off-axis at 9°48'N are consistent with up to 15% melt in films or tubes. Melt in thin sills would require a much higher melt percentage for the same shear velocity.

At all near-axis sites (<0.6 km from the rise axis), compliances at lower crustal frequencies are high enough to indicate mush, suggesting that the central mush zone is continuous and that the near-axis lower crust is highly permeable. At all of the measurement sites, lower crust shear velocities are slower than the 3.4–4 km/s found in old Pacific lower crust [21], indicating that tempera-

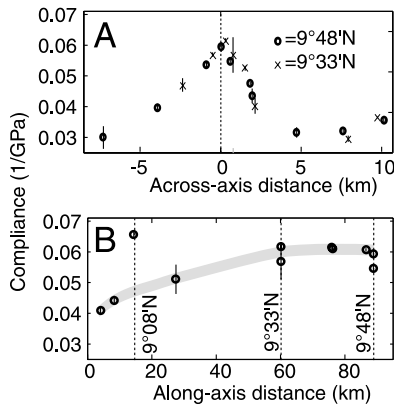


Fig. 5. Across- and along-axis variations in 10-mHz compliance. (A) $9^{\circ}48'N$ and $9^{\circ}33'N$ data plotted together as a function of distance from the rise axis. The $9^{\circ}33'N$ data are shifted 0.7 km east with respect to the axial summit collapse trough (as imaged by [28]). (B) Data from all near-axis sites (<0.6 km off-axis) as a function of distance along the rise axis. Grey region highlights the general trend; dotted lines mark the across-axis compliance measurement lines.

tures and/or porosity are high throughout the survey area.

The width, shape, and alignment of the central mush zone can be inferred from the shape of the peak in 10-mHz compliance versus distance from the rise axis (Fig. 4B). From $9^{\circ}48'N$ to $9^{\circ}22'N$, we consider the rise axis to be at the center of the axial summit collapse trough [23], which marks the center of surface magmatism and hydrothermalism [24]. South of $9^{\circ}22'N$, we use the distance from the axial bathymetric high. At $9^{\circ}48'N$ and at $9^{\circ}33'N$, the 10-mHz compliance peak is 5–8 km wide. Seismic tomography data image a 4–6-km-wide mush zone at $9^{\circ}33'N$ [14], so the peak width appears to give an adequate estimate of the mush zone width. This peak has the same shape at $9^{\circ}48'N$ and $9^{\circ}33'N$ (Fig. 5A), indicating that the mush zones are very similar. The peak decreases more rapidly to the east than to the west, indicating that the mush zone is asymmetric, with more melt to the west. In addition, the mush zone shifts west of the rise axis between $9^{\circ}48'N$ and $9^{\circ}33'N$. At $9^{\circ}48'N$, the maximum compliance is at the rise axis, whereas at $9^{\circ}33'N$ the maximum is 0.5–1 km west of the rise axis. To align the $9^{\circ}33'N$ compliance with the $9^{\circ}48'N$ compliance in Fig. 5A, the

$9^{\circ}33'N$ compliance values had to be shifted 0.7 km east with respect to the rise axis. The misalignment of this mush zone is also suggested by seismic tomography [14,25] but the asymmetry is only suggested in the compliance data, indicating that compliance is more sensitive to lateral variations on the km scale. The compliance data do not detect the high velocities at the base of the crust imaged by seismic tomography [14], perhaps because seismic rays are more sensitive than compliance to the vertical velocity gradient [18] or because of anisotropic velocity changes with depth that may not be associated with a change in melt percentage [16].

The $9^{\circ}08'N$ line crosses the rise axis at the northern limit of the $9^{\circ}N$ OSC. The central mush zone is much broader here than at the two northern lines (Fig. 4A,B). Compliance again decreases rapidly to the east of the rise axis, but it

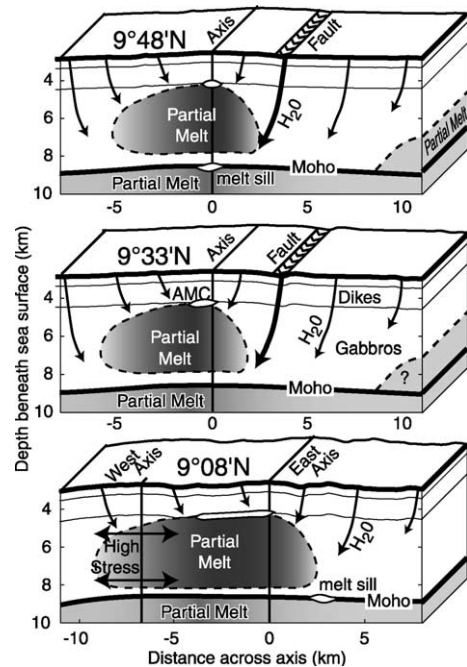


Fig. 6. Interpretative EPR cross sections based on compliance and seismic data. Major features include an AMC reflector, Moho melt sills, a central mush zone and off-axis lower crust mush zones. Darker shading indicates more melt, curved arrows indicate hydrothermal fluid penetration, and horizontal arrows indicate high stress.

remains high out to 6–8 km west of the rise axis, spanning the distance between the east and west limbs of the OSC. Compliance and seismic data indicate that this is a local anomaly. The high on-axis compliance value at 9°08'N is the only break in a trend of decreasing compliance towards the OSC (Fig. 5B), and seismic tomography reveals an isolated lower crustal LVZ at both the northern and southern OSC limits [26].

3. Discussion

Fig. 6 shows a model of the melt distribution beneath the EPR from 9° to 10°N, derived both from the compliance results and from previous seismic reflection and refraction studies. The AMC width and location come from seismic reflection studies [4,5], the lower crustal melt distribution comes from our compliance data and seismic tomography results [14,25] and the melt at the top of the mantle comes from seismic data [17]. In the lower crust, the compliance data best constrain the melt zone's horizontal asymmetry and its offset from the rise axis, while the seismic results indicate that most of the melt lies in the upper half of the lower crust ([14], but this could also be the result of a change in the melt geometry with depth [16]).

3.1. The central lower crustal melt zone (CMZ)

At 9°33' and 9°48'N, the CMZ is asymmetric, extending further west than east of the maximum melt region. Variations in compliance with distance across-axis are identical at these two latitudes, suggesting that the amount and distribution of lower crustal melt is also identical, even though the ridge has a more 'inflated' appearance and has been more volcanically active at 9°48'N [27,28]. At 9°48'N, the maximum compliance is at the rise axis, while at 9°33'N the maximum is offset 0.5–1.0 km west of the axis. The CMZ is much wider at 9°08'N, where a 7–10-km-wide region of near-maximum 10-mHz compliances spans the gap between the two OSC limbs.

Seismic tomography data indicating that CMZ velocities increase with depth have been inter-

preted as indicating that most of the melt is near the top of the lower crust. Studies of foliation in the Oman ophiolite suggest, however, that CMZ melt is abundant throughout the lower crust and that it does not decrease with depth [16]. These studies suggest that the apparent seismic velocity increases with depth because of changes in the melt geometry. Furthermore, these velocity changes are anisotropic, meaning that the gradient visible in seismic tomography data might not exist in the strain direction that compliance measurements are sensitive to.

The CMZ probably contains more melt than the AMC. Lower crustal shear velocities below 2 km/s are required at all eight near-axis compliance measurement sites between the OSC and 9°48'N, suggesting that the CMZ is continuous along-axis. The CMZ is therefore probably the most volumetrically important crustal melt reservoir. The minimum possible melt in the CMZ (2.5%) summed over 4 km of lower crust adds up to as much melt as a fully molten, 100-m-tall AMC of the same width [14,18]. Since the CMZ is wider than the AMC and it probably averages more than 2.5% melt, it contains significantly more melt than the AMC. It remains to be determined how much of the lower crustal melt passes to the AMC and the upper crust but the CMZ would play an important role in crustal accretion even if all of its melt froze in place in the lower crust. The alignment of the AMC with the CMZ (discussed below) suggests, however, that it also contributes to the creation of the upper crust.

Morphological models (e.g. [27]) and geochemical data (e.g. [29]) indicate that the melt supply is more robust beneath the axial bathymetric high at 9°50'N than at the bathymetric low at the 9°03'N OSC. Our compliance data show no evidence of a corresponding decrease in lower crustal melt south of 9°48'N. The central mush zone appears identical at 9°48'N and at 9°33'N and contains the most melt at 9°08'N. 10-mHz compliance amplitudes do decrease south of 9°48'N (except at 9°08'N), indicating an increase in lower crustal shear velocities, but the decrease is quite small and could be associated with a shift of the central mush body west of the rise axis.

3.2. *The off-axis lower crustal melt zone at 9°48'N*

At 9°48'N, a separate lower crustal melt zone begins approximately 10 km east of the rise axis and extends to at least 14 km off-axis. The melt in this zone is concentrated near the bottom of the lower crust. We do not have enough off-axis compliance measurements to determine if this zone extends farther off-axis, if the zone is continuous along-axis, or if there is a corresponding zone 10+ west of the rise axis. Our farthest off-axis measurements are 14 km east and 7 km west of the rise axis at 9°48'N and 3–9 km off-axis at other latitudes. Nevertheless, lower crustal shear velocities do decrease with distance off-axis at the farthest off-axis sites at 9°33'N and 9°08'N (Fig. 4C), suggesting that the off-axis melt zone at 9°48'N may not be an isolated feature.

3.3. *Lower crustal and Moho melt sills*

Studies of the Oman ophiolite indicate that the near-axis lower crust may contain one or more melt sills [12,30]. Our compliance measurements do not detect any such sills beneath the EPR. They do not rule out their presence, either, but they indicate that, if they do exist, they are too small or have too high velocity to create separately identifiable compliance peaks. The presence of lower crustal melt sills or pockets could have important consequences for the interpretation of seismic and compliance data, especially if the melt bodies are isolated from one another. Seismic tomography data indicate that on-axis lower crustal velocities increase towards the Moho. The usual interpretation of this velocity profile is that melt is concentrated near the top of the lower crust [14], but the same profile could be created by a change in melt geometry with depth. Melt in isolated bodies is much less efficient at reducing bulk velocities than are connected films or tubes [31]. Similarly, small-scale isolated bodies such as sills could be missed as seismic energy refracts around such bodies. Seismic velocities could therefore increase with depth for a constant melt percentage if melt exists mostly in grain-scale or larger isolated bodies near the bottom of the lower crust

and in connected films or tubes at the grain scale near the top.

Studies of the Oman ophiolite also indicate that a particularly large sill (or sills) may reside at or near the Moho [12,30]. These may correspond to the melt bodies detected at approximately Moho depth beneath four of our measurement sites. One of these melt bodies (at 9°08'N) lies 2.5 km east of the rise axis (Fig. 1). This body lies within the tomographically imaged melt region in the uppermost mantle [17] but sits 8–10 km east of the region's center (where the minimum velocities are located), suggesting that it was not created at the focus of mantle upwelling. Its distance from the AMC also suggests that it does not feed the AMC (or at least not from directly below). Moho melt bodies may be created by asperities in the upper mantle melt zone or by gravitational focusing of melt to local highs in Moho topography [32]. It is unclear how important a role they play in melt differentiation and crustal genesis, but they do appear to be common beneath this EPR segment.

The sensitivity of compliance measurements to Moho melt bodies but not to the upper mantle LVZ highlights how compliance and seismic measurements complement each other. Seismic measurements can detect and constrain the diffuse upper mantle LVZ but are insensitive to melt sills because seismic rays diffract around small, low-velocity bodies. The compliance measurements, on the other hand, detect the sills because of their near-zero shear velocity but are insensitive to the relatively small velocity anomaly of the upper mantle LVZ.

3.4. *Alignment of the CMZ with other melt regions*

The AMC [5], CMZ and upper mantle melt zone are all aligned beneath the rise axis at 9°48'–50'N and they all shift westward relative to the rise axis towards the 9°03'N OSC. Moreover, to within the precision of the measurements used to determine their positions, the west edge of the AMC is aligned with the centers of both the CMZ and the upper mantle melt zone. At 9°48'N the CMZ and the AMC are both centered beneath the rise, while at 9°33'N the center of the

CMZ and the western edge of the AMC sit 0.5–1 km west of the rise axis. The upper mantle melt zone is centered beneath the rise axis at 9°48'N and appears to be offset slightly west at 9°33'N, although the resolution uncertainty is greater than 1 km [17]. At 9°08'N, the upper mantle melt zone is centered 5–7 km west of the rise axis and the CMZ and AMC appear to follow. The situation is rather complicated, however: the CMZ extends 7–10 km west of the rise axis but the focus of its melting is 1 km west of the rise axis, while the AMC extends 4 km west of the rise axis.

Kent et al. [5] proposed that, where the AMC is offset from the rise axis, it transports magma to the rise axis from an off-axis 'line' source. Our data support the essence of their theory but indicate that the AMC more likely feeds off of the center of the lower crustal mush zone instead of a line source directly from the mantle. Our data also support an important consequence of their theory: that the width of the AMC depends on the alignment of deep melt with the rise axis, not on the amount of melt supplied.

3.5. *Explanations for the size and shape of the lower crustal melt region*

The compliance measurements demonstrate that, although the CMZ and the upper mantle melt zone are aligned, the CMZ is much narrower than the mantle melt zone inferred from seismic tomography. It is not understood why the CMZ is so narrow. Simple conductive cooling models (e.g. Parker and Oldenburg [33]) predict a CMZ more than 20 km wide under fast-spreading ridges such as the EPR. The CMZ must either be much wider than indicated by the seismic velocities or the lower crust must be cooled by a process much more efficient than conduction in a simple non-convecting plate spreading model. We will discuss these two possibilities below.

It is possible that the lower crustal melt region is wider than the seismic velocities indicate, if the velocities are primarily controlled by the melt geometry rather than the total melt percentage. For example, 7% melt reduces shear velocities by 40% if the melt is in connected thin films or tubes and by only 7% if the melt is stored in isolated spheres

[20]. The observed velocity variations might therefore be explainable by a change from connected melt on-axis to isolated melt off-axis as thin connecting melt bodies freeze first under slow (conductive) cooling. This model does not explain why there would be a renewal of connected melt 10 km off-axis, nor does it explain the asymmetry of the CMZ beneath the ridge axis.

Alternative models require that the crust is partly cooled by convective processes: by hydrothermal circulation deep into the crust, by convection within a magma chamber, or by both.

Hydrothermal circulation that penetrates most of the crust off-axis has previously been invoked to explain the narrow width of the CMZ [14,34]. It can also provide an explanation for both the asymmetry of the central melt zone and the existence of off-axis melt. Deep hydrothermal circulation could create asymmetric melt zones at 9°48'N and 9°33'N through asymmetric near-axis crustal faulting that allows more efficient cooling east of the rise axis. The seafloor is more rugged and deepens more rapidly to the east, with deep fault grabens 3–4 km east of the rise axis [35] providing potentially efficient pathways for deep hydrothermal circulation and cooling. Dunn et al. [17] observe that the asymmetry could be caused by the offset of the ridge axis to the east of the mantle upwelling, but we observe this asymmetry as far north as 9°48'N, where the ridge appears to be aligned with the upper mantle melt.

The reappearance of melt 10 km off-axis may be explained by a rapid decrease in deep hydrothermal circulation with distance off-axis. Heat flux and geochemical measurements put an upper age limit of 5–10 Myr (250–600 km) on crustal hydrothermalism [36,37], but vigorous deep circulation may be limited to a much narrower region. In fact, near-axis subsidence rates indicate that vigorous lower crustal cooling is limited to a region 3–7 km from the rise axis [38], which corresponds well with the region where compliance measurements indicate the highest lower crustal shear velocities. Possible reasons for the rapid decrease in deep circulation include pressure sealing of cracks, permeability changes due to mineral diagenesis [39] and reduction of overall flow due to surface sedimentation. Deeply penetrating hy-

drothermal systems within a few kilometers of the rise axis might be detected by the presence of off-axis vents or by the seismicity they might induce, but there is as yet little evidence of either.

The hydrothermal cooling model might also help explain why the EPR neovolcanic zone is only 1–2 km wide despite a wider mantle melt supply [17,40–42]. Vigorous deep hydrothermal circulation in the near-axis crust may inhibit melt from rising to the surface between approximately 2–8 km from the rise axis, limiting most eruptions to a narrow axial zone and to off-axis sites. The distance off-axis at which local seamount chains begin (6–15 km [43]) may be controlled by the off-axis limit of deep hydrothermal cooling.

The problem with the deep hydrothermal cooling model is that there exists little evidence for off-axis vents or the seismicity that might be induced by rapidly cooling a thick crustal section. Without hydrothermal cooling, one must invoke convection within the lower crustal magma chamber to solidify the lower crust within a few kilometers of the rise axis. This convection could be very slow, as in the ‘gabbro glacier’ or ‘conveyor belt’ models [7,44] where cumulates fall out onto the bottom of a rapidly cooled melt lens, then ductilely deform during extension to form the lower crust. The Oman ophiolite lower crust is divided into two layers: a bottom layer of modally layered gabbros known as the ‘lower’ or ‘layered’ gabbros and an upper section of non-layered gabbros known as the ‘foliated gabbros’ or the ‘mid-crust’. The layered gabbros show predominantly flat layering that is best explained by the emplacement of sill sequences [45] and that is inconsistent with the pervasive deformation required by convective models. This suggests that any lower crustal convection is limited to the mid-crust [30].

Convective cooling in the mid-crustal magma chamber could allow the CMZ to essentially freeze within a few kilometers of the rise axis. The layered gabbros would be constructed under the rise axis by periodic injection of sills [44] in a thermal boundary layer with heat extracted by convection in the mid-crust. The width of the CMZ would be controlled by this convection

and by the amount of melt percolating in from below and therefore by the permeability of the crust mantle transition zone as suggested by Kelemen and Aharonov [44]. A broad lens of dense, olivine-rich melt is expected to pool at the crust/mantle boundary under this permeability cap, which we associate with the upper mantle anomaly inferred from seismic tomography.

In this model the east–west asymmetry of the topography adjacent to the rise axis would not control crustal magmatism but rather the opposite. A lower melt fraction and cooler lower crust east of the rise axis would generate a more faulted, rugged terrain than above the melt-rich lower/mid crust to the west. The reappearance of melt in the lower crust 10 km off-axis would be a consequence of lower crustal reheating from below after the overlying convective cooling is removed as the mid-crust fully freezes.

3.6. *The 9°08′N melt anomaly: more crustal control of the shape of the CMZ?*

The wide melt region at 9°08′N appears to be another case of a crustal process controlling the lower crustal melt distribution. This melt region sits at the northern tip of the 9°03′N OSC, where crustal stress should be strong but beneath which there is no reason to expect enhanced mantle upwelling. Crustal extensional and shear stresses near OSC tips are 3–4 times stronger than normal [46], and stress-induced cracking and deformation may allow melt to penetrate from the 15–20-km-wide mantle melt zone [17] into a wider-than-normal section of the crust. A 3-D seismic refraction study of the 9°03′N OSC images low-velocity anomalies in the lower crust at both the northern and southern OSC tips, providing further evidence that this anomaly is tied to the OSC tips and therefore to crustal processes. In contrast, imaged upper mantle melt is not enhanced beneath the OSC tips [17].

3.7. *Unanswered questions*

The greater fractionation of surficial axial basalts towards the 9°03′N OSC and the 10°10′N transform than at 9°50′N has been interpreted

as indicating that melt spreads south and north from a focus near 9°50'N [29]. The compliance data do not reveal any along-axis velocity variations supporting this model. If we do not see this segmentation in the lower crust, where do the geochemical variations come from? Whole segment flow seems unlikely in the AMC, since the AMC appears to mostly contain a crystal mush rather than pure melt [19], because significant along-axis flow is contradicted by rapid variations observed in the AMC width [10] and because recent geochemical data suggest that any segmentation is discrete [24]. There is no evidence for segmentation in the mantle, either, since velocity anomalies at the top of the mantle indicate as much melt at the OSC as at 9°20–30'N [14,17], and deeper mantle variations seem unlikely since they should affect at least the upper mantle melt distribution. Perhaps the greater surficial basalt fractionation in the OSC's eastern limb is the result of the AMC's greater width or of the tapering out of the AMC as the melt supply shifts to the OSC's western limb. Alternatively, along-axis velocity changes associated with changes in melt supply may be too subtle for the seismic and compliance data to detect (the 0.1 km variation in the depth to the rise axis over the 100-km-segment length is, after all, fairly subtle). Finally, this segment may be in a temporary phase of linear melt supply.

Our compliance experiment, combined with information from seismic studies [5,14,17,25], suggests that, while the mantle melt supply controls the existence and location of crustal melt, crustal processes provide the final control on the size and shape of the CMZ. Our results also suggest that crustal melt may extend much farther off-axis than previously believed, both in the form of a central melt zone that is offset from the rise axis and in separate melt regions that begin several kilometers off-axis. More off-axis studies may be necessary to determine the distribution and role of melt beneath fast-spreading oceanic ridges.

Acknowledgements

The compliance data was collected during night operations during three cruises on the R/V *Atlan-*

tis and the R/V *New Horizon*. We thank the captain, crew and scientific party of both ships for their tireless help and the gentle care they provided for the compliance sensors. We thank Craig Cary, Chuck Fisher, Lauren Mullineaux and Rob Evans for allowing us to measure compliance during their expeditions. The compliance sensors exist and function thanks to the engineering and logistical efforts of Jacques Lemire and Tom Deaton. Daniel Doherty capably assisted with all of the sensor launches and recoveries as well as acoustic surveys, instrument repairs and pre-cruise instrument preparation. Dan Fornari's timely aid helped us to overcome last-minute logistic problems. Peter Kelemen and Marc Spiegelman provided fruitful discussions and comments on the manuscript, and we thank Robert Dunn and Mike Perfit for thoughtful and insightful reviews. This research was funded by NSF grants OCE9819159 and OCE0002878. **[BOYLE]**

Appendix. Measurement and inversion of compliance data

We measure seafloor compliance by deploying an autonomous instrument containing a broadband seismometer and pressure gauge to the seafloor for 2–3 days, then calculating the transfer function between displacement and pressure as a function of frequency using 1024-s windows [47]. Compliance is inversely proportional to the shear modulus [47], making it particularly sensitive to the existence of fluids. The ocean surface gravity waves that create the compliance signal travel much slower than most seismic waves, so the compliance measurements are quasi-static and are not limited by diffraction or attenuation in melt-rich regions.

The depth of compliance sensitivity is proportional to the forcing wavelength, which decreases with increasing frequency, so compliance is sensitive to deep structure at low frequencies and to shallow structure at high frequencies [47,48]. At the EPR, compliance is most sensitive to the upper crust (depths shallower than 1.5 km) at frequencies above 14 mHz, to the AMC between 13 and 14 mHz, to the lower crust (depths

between 1.5 and 6 km) between 8 and 12 mHz, and to the Moho and upper mantle below 8 mHz [18].

To calculate shear velocities from compliance measurements, we use a 1-D minimum structure inversion [49] or 1- and 2-D block inversions [18]. We use the minimum structure inversions to determine if the data require structural anomalies, and the block inversions to find the best-fitting shear velocities. For the block models, we use boundary depths from seismic reflection and refraction data [4,5,50–52] to divide a 1- or 2-D EPR model into discrete blocks: seismic layers 2A, 2B and 3, the mid-crustal melt lens and, if necessary, a deep melt lens. We then determine the best-fitting velocity or velocity ratio in each block using genetic and grid-search algorithms. Although 2-D block models are more realistic, they are also more biased by our assumptions about the lateral rate of change of velocities within a block. 1-D block models, on the other hand, assume that there is no lateral change and provide the most conservative velocity estimates at sites where compliance is locally maximum or minimum. In this paper, we present these conservative estimates from 1-D block model inversions at maximum and minimum compliance sites indicated by ‘N’, ‘I’ and ‘F’ in Fig. 4. The actual velocities may be lower in the near and far regions and higher in the intermediate region.

The inversions and data calculations return the shear modulus (μ), but for easier comparison with seismic data we convert to shear velocity (V_s) using the formula $V_s = \sqrt{\mu/\rho}$, where ρ is the density. Since density varies much less than the shear modulus/velocity, we can use typical crust and mantle densities without significant error.

Compliance is nearly insensitive to layer 2A velocities because the layer is relatively thin and the data uncertainty is highest at the frequencies sensitive to this layer [18]. To estimate the effect of inaccuracies in the thickness of layer 2B and the lower crust, we also calculated shear velocities using models with anomalously thick and thin layer 2B and lower crust. Thickness variations of ± 0.5 km in layer 2B and ± 1 km in the lower crust have no significant effect on the results.

References

- [1] E.M. Moores, F.J. Vine, The Troodos Massif, Cyprus and other ophiolites as oceanic crust: evaluation and implications, *Philos. Trans. R. Soc. Lond. A* 268 (1971) 443–466.
- [2] J.M. Sinton, R.S. Detrick, Mid-ocean ridge magma chambers, *J. Geophys. Res.* 97 (1992) 197–216.
- [3] R.S. Detrick, P. Buhl, E. Vera, J. Mutter, J. Orcutt, J. Madsen, T. Brocher, Multi-channel seismic imaging of a crustal magma chamber along the East Pacific Rise, *Nature* 326 (1987) 35–41.
- [4] G.M. Kent, A.J. Harding, J.A. Orcutt, Distribution of magma beneath the East Pacific Rise between the Clipperton Transform and the 9°17'N deval from forward modeling of common depth point data, *J. Geophys. Res.* 98 (1993) 13945–13969.
- [5] G.M. Kent, A.J. Harding, J.A. Orcutt, Distribution of magma beneath the East Pacific Rise near the 9°03'N overlapping spreading center from forward modeling of common depth point data, *J. Geophys. Res.* 98 (1993) 13971–13995.
- [6] M. Tolstoy, A.J. Harding, J.A. Orcutt, T. Group, Deepening of the axial magma chamber on the southern East Pacific Rise toward the Garrett Fracture Zone, *J. Geophys. Res.* 102 (1997) 3097–3108.
- [7] J.E. Quick, R.P. Denlinger, Ductile deformation and the origin of layered gabbro in ophiolites, *J. Geophys. Res.* 98 (1993) 14015–14027.
- [8] W.R. Buck, S.M. Carbotte, C. Mutter, Controls on extrusion at mid-ocean ridges, *Geology* 25 (1997) 935–938.
- [9] Y.J. Chen, J. Phipps Morgan, The effects of spreading rate, the magma budget, and the geometry of magma emplacement on the axial heat flux at mid-ocean ridges, *J. Geophys. Res.* 101 (1996) 11475–11482.
- [10] G.M. Kent, S.C. Singh, A.J. Harding, M.C. Sinha, J.A. Orcutt, P.J. Barton, R.S. White, S. Bazin, R.W. Hobbs, C.H. Tong, J.W. Pye, Evidence from three-dimensional seismic reflectivity images for enhanced melt supply beneath mid-ocean-ridge discontinuities, *Nature* 406 (2000) 614–618.
- [11] J.H. Natland, H.J.B. Dick, Melt migration through high-level gabbroic cumulates of the East Pacific Rise at Hess Deep: the origin of magma lenses and the deep crustal structure of fast-spreading ridges, in: C. Mével, K.M. Gillis, J.F. Allan, et al. (Eds.), *Proceedings of the Ocean Drilling Program, Scientific Results*, vol. 147, Ocean Drilling Program, College Station, TX, 1996, pp. 21–58.
- [12] P.B. Kelemen, K. Koga, N. Shimizu, Geochemistry of gabbro sills in the crust-mantle transition zone of the Oman Ophiolite; implications for the origin of the oceanic lower crust, *Earth Planet. Sci. Lett.* 146 (1997) 475–488.
- [13] W.S.D. Wilcock, S.C. Solomon, G.M. Purdy, D.R. Toomey, Seismic attenuation structure of the East Pacific Rise near 9 degrees 30'N, *J. Geophys. Res.* 100 (1995) 24147–24165.
- [14] R.A. Dunn, D.R. Toomey, S.C. Solomon, Three-dimen-

- sional seismic structure and physical properties of the crust and shallow mantle beneath the East Pacific Rise at 9 degrees 30'N, *J. Geophys. Res.* 105 (2000) 23537–23556.
- [15] E. Aharonov, M. Spiegelman, P. Kelemen, Three-dimensional flow and reaction in porous media: implications for the Earth's mantle and sedimentary basins, *J. Geophys. Res.* 102 (1997) 14821–14833.
- [16] G. Lamoreux, B. Ildefonse, D. Mainprice, Modelling the seismic properties of fast-spreading ridge crustal low-velocity zones: insights from Oman gabbro textures, *Tectonophysics* 312 (1999) 283–301.
- [17] R.A. Dunn, D.R. Toomey, R.S. Detrick, W.S.D. Wilcock, Continuous mantle melt supply beneath an overlapping spreading center on the East Pacific Rise, *Science* 291 (2001) 1955–1958.
- [18] W.C. Crawford, S.C. Webb, J.A. Hildebrand, Constraints on melt in the lower crust and Moho at the East Pacific Rise, 9°48'N, using seafloor compliance measurements, *J. Geophys. Res.* 104 (1999) 2923–2939.
- [19] S.C. Singh, G.M. Kent, J.S. Collier, A.J. Harding, J.A. Orcutt, Melt to mush variations in crustal magma properties along the ridge crest at the southern East Pacific Rise, *Nature* 394 (1998) 874–878.
- [20] G.M. Mavko, Velocity and attenuation in partially molten rocks, *J. Geophys. Res.* 85 (1980) 5173–5189.
- [21] P. Spudich, J. Orcutt, A new look at the seismic velocity structure of the oceanic crust, *Rev. Geophys. Space Phys.* 18 (1980) 627–645.
- [22] H. Schmeling, Numerical models on the influence of partial melt on elastic, anelastic and electric properties of rocks; Part 1: elasticity and anelasticity, *Phys. Earth Planet. Inter.* 41 (1985) 34–57.
- [23] R.M. Haymon, D.J. Fornari, M.H. Edwards, S. Carbotte, D. Wright, K.C. MacDonald, Hydrothermal vent distribution along the East Pacific Rise crest (9 degrees 09'–54'N) and its relationship to magmatic and tectonic processes on fast-spreading mid-ocean ridges, *Earth Planet. Sci. Lett.* 104 (1991) 513–534.
- [24] M.C. Smith, M.R. Perfit, D.J. Fornari, W.I. Ridley, M.H. Edwards, G.J. Kurras, K.L.V. Damm, Magmatic processes and segmentation at a fast spreading mid-ocean ridge: detailed investigation of an axial discontinuity on the East Pacific Rise crest at 9°37'N, G-cubed 2(2000GC000134), 2001.
- [25] D.R. Toomey, G.M. Purdy, S.C. Solomon, W.S.D. Wilcock, The three-dimensional seismic velocity structure of the East Pacific Rise near latitude 9 degrees 30' N, *Nature* 347 (1990) 639–645.
- [26] S. Bazin, Three-dimensional crustal structure of East Pacific Rise discontinuities from tomographic inversions, Ph.D. thesis, UC San Diego, CA, 2000.
- [27] K.C. Macdonald, P.J. Fox, L.J. Perram, M.F. Eisen, R.M. Haymon, S.P. Miller, S.M. Carbotte, M.H. Cormier, A.N. Shor, A new view of the mid-ocean ridge from the behaviour of ridge-axis discontinuities, *Nature* 335 (1988) 217–225.
- [28] D.J. Fornari, R.M. Haymon, M.R. Perfit, T.K.P. Gregg, M.H. Edwards, Axial summit trough of the East Pacific Rise 9°–10°N: geological characteristics and evolution of the axial zone on fast spreading mid-ocean ridges, *J. Geophys. Res.* 103 (1998) 9827–9855.
- [29] R. Batiza, Magmatic segmentation of mid-ocean ridges: a review, in: C.J. MacLeod, P.A. Tyler, C.L. Walker (Eds.), *Tectonic, Magmatic, Hydrothermal and Biological Segmentation of Mid-Ocean Ridges*, Geol. Soc. Spec. Publ. 118, The Geological Society, London, 1996, pp. 103–130.
- [30] F. Boudier, A. Nicolas, Magma chambers in the Oman Ophiolite; fed from the top and bottom, *Earth Planet. Sci. Lett.* 144 (1996) 239–250.
- [31] G. Mavko, T. Mukerji, J. Dvorkin, *The Rock Physics Handbook: Tools for Seismic Analysis in Porous Media*, Cambridge University Press, Cambridge, 1998, 330 pp.
- [32] J. Garmany, Correlation of bathymetry and melt location near the East Pacific Rise at 9 degrees 30'N, *Eos Trans. AGU* 76 (1995) F595.
- [33] R.L. Parker, D.W. Oldenburg, Thermal model of ocean ridges, *Nat. Phys. Sci.* 242 (1973) 137–139.
- [34] J. Phipps Morgan, Y.J. Chen, The genesis of oceanic crust: magma injection, hydrothermal circulation, and crustal flow, *J. Geophys. Res.* 98 (1993) 6283–6297.
- [35] K.C. Macdonald, P.J. Fox, R.T. Alexander, R. Pockalny, P. Gente, Volcanic growth faults and the origin of Pacific abyssal hills, *Nature* 380 (1996) 125–129.
- [36] S.R. Hart, H. Staudigel, Oceanic crust: age of hydrothermal alteration, *Geophys. Res. Lett.* 5 (1978) 1009–1012.
- [37] I. Grevmeyer, N. Kaul, H. Villinger, W. Weigel, Hydrothermal activity and the evolution of the seismic properties of upper oceanic crust, *J. Geophys. Res.* 104 (1999) 5069–5079.
- [38] J.R. Cochran, W.R. Buck, Near-axis subsidence rates, hydrothermal circulation, and thermal structure of mid-ocean ridge crests, *J. Geophys. Res.* 106 (2001) 19233–19258.
- [39] F.J. Fontaine, M. Rabinowicz, J. Boulègue, Permeability changes due to mineral diagenesis in fractured crust: implications for hydrothermal circulation at mid-ocean ridges, *Earth Planet. Sci. Lett.* 184 (2000) 407–425.
- [40] J. Phipps Morgan, Melt migration beneath mid-ocean spreading centers, *Geophys. Res. Lett.* 14 (1987) 1238–1241.
- [41] M. Spiegelman, Geochemical consequences of melt transport in 2-D: The sensitivity of trace elements to mantle dynamics, *Earth Planet. Sci. Lett.* 139 (1996) 115–132.
- [42] H. Zou, A. Zindler, Y. Niu, Constraints on melt movement beneath the East Pacific Rise from ²³⁰Th–²³⁸U disequilibrium, *Science* 295 (2002) 107–110.
- [43] D.S. Scheirer, K.C. Macdonald, Near-axis seamounts on the flanks of the East Pacific Rise, 8 degrees N to 17 degrees N, *J. Geophys. Res.* 100 (1995) 2239–2259.
- [44] P.B. Kelemen, E. Aharonov, Periodic formation of magma fractures and generation of layered gabbros in the lower crust beneath oceanic spreading ridges, in: W.R. Buck, P.T. Delaney, J.A. Karson, et al. (Eds.), *Faulting*

- and Magmatism at Mid-Ocean Ridges, *Geophys. Monogr.* 106, Am. Geophys. Union, Washington, DC, 1998, pp. 267–289.
- [45] J. Korenaga, P.B. Kelemen, Origin of gabbro sills in the Moho transition zone of the Oman ophiolite: Implications for magma transport in the oceanic lower crust, *J. Geophys. Res.* 102 (B12) (1997) 27729–27749.
- [46] D.D. Pollard, A. Aydin, Propagation and linkage of oceanic ridge segments, *J. Geophys. Res.* 89 (1984) 10017–10028.
- [47] W.C. Crawford, S.C. Webb, J.A. Hildebrand, Seafloor compliance observed by long-period pressure and displacement measurements, *J. Geophys. Res.* 96 (1991) 16151–16160.
- [48] W.C. Crawford, S.C. Webb, J.A. Hildebrand, Estimating shear velocities in the oceanic crust from compliance measurements by two-dimensional finite difference modeling, *J. Geophys. Res.* 103 (1998) 9895–9916.
- [49] S.C. Constable, R.L. Parker, C.G. Constable, Occam's inversion a practical algorithm for generating smooth models from electromagnetic sounding data, *Geophysics* 52 (1987) 289–300.
- [50] A.J. Harding, G.M. Kent, J.A. Orcutt, A multichannel seismic investigation of upper crustal structure at 9 degrees N on the East Pacific Rise: implications for crustal accretion, *J. Geophys. Res.* 98 (1993) 13925–13944.
- [51] G.A. Barth, J.C. Mutter, Variability in oceanic crustal thickness and structure: Multichannel seismic reflection results from the northern East Pacific Rise, *J. Geophys. Res.* 101 (1996) 17951–17975.
- [52] J.S. Collier, S.C. Singh, Detailed structure of the top of the melt body beneath the East Pacific Rise at 9 degrees 40'N from waveform inversion of seismic reflection data, *J. Geophys. Res.* 102 (1997) 20287–20304.